Birjand University of technology

Faculty of Mechanical and Materials Engineering

In the Name of God, the Most Gracious, the Most Merciful

Bachelor's Thesis in Mechanical Engineering

Title: Aluminum Composite Sheets

Student: Alireza Jokar (9713611113)

Supervisor: Dr. Seyed Ehsan Eftekhari

Summer 2022

Abstract

In Paper 1, roll bonding, which is a solid-state welding process, is used to create bonding between a wide range of metals through a simple rolling operation. In this study, a multilayer aluminum–magnesium composite consisting of Al 5052 and AZ31B was fabricated using the roll bonding process, and its formability was evaluated. The rolling process was carried out at room temperature with a thickness reduction of 70%. Forming limit diagrams (FLDs), which are commonly used to assess the formability of sheet metals, were employed to determine the limiting strains prior to fracture and necking. The mechanical property results also showed that, due to cold working and the increase in dislocation density, the strength and microhardness of the aluminum/magnesium multilayer composite improved by 149.5% and 80%, respectively, compared with the initial aluminum.

In Paper 2, the surface of SPF aluminum sheet (7075-T6) was reinforced with pumice microparticles and nanoparticles using the friction stir processing (FSP) method. First, the optimal processing conditions in terms of the number of passes (1 and 4 passes), linear travel speed (40 and 80 mm/min), and tool rotational speed (800 and 1200 rpm) were selected based on the microstructure, hardness, and wear resistance of aluminum. The results indicated that increasing the number of passes, decreasing the linear travel speed, and increasing the tool rotational speed led to a reduction in grain size in the stirred zone, as well as increases in hardness and wear resistance. By adding pumice microparticles and nanoparticles to the aluminum matrix, the average hardness increased to 99.6 and 107.8 Vickers, respectively, while the wear loss decreased to 24 and 20 mg, respectively.

Table of Contents

Title Page

**Chapter 1: Summary of Paper 1 entitled

(Investigation of the Forming Limit of Multilayer Composites Processed by the Roll Bonding Method)

1-1 Introduction …… 1

1-2 Cold Roll Bonding Process ……..… 1

1-3 Forming Limit Diagrams …… 3

1-4 Plastic Instability ……. 5

1-5 Results and Discussion …… 5

1-6 Fracture Analysis … ……6

1-7 Mechanical Properties ……..8

1-8 Formability ……..… 9

**Chapter 2: Summary of Paper 2 entitled

“Fabrication and Surface Reinforcement of 7075 Aluminum Using Pumice Micro- and Nanoparticles via the Friction Stir Processing (FSP) Method

2-1 Introduction ……... 11

2-2 Materials and Experimental Procedure ……..… 12

2-3 Results and Discussion … ……..14

Chapter 3

Introduction to Composites and Aluminum Composites, Their Applications and Characteristics …… 17

Chapter 4

Methods for Fabrication of Aluminum Composites ……... 20

Chapter 5

Conclusion ……..… 22

References ……...… 23

Chapter 1

1-1 Introduction

In this paper, a composite consisting of aluminum and magnesium is investigated. These materials are very lightweight and have lower density compared to other alloys. Moreover, aluminum–magnesium laminated composites are widely used due to their excellent properties such as low density, high strength, and good corrosion resistance.

Among the existing technologies for composite fabrication, the cold roll bonding method is considered the most suitable due to its simplicity. Another related technique is roll welding, in which surface preparation and appropriate thickness reduction are essential parameters for the process. Since this method is performed at ambient temperature, it results in favorable mechanical properties and good strength improvement (up to two times).

1-2 Cold Roll Bonding Process

According to Figure 1, the initial samples were cut to identical dimensions of 125 mm in length and 70 mm in width, with thicknesses of 2 mm and 1.5 mm for aluminum and magnesium, respectively.

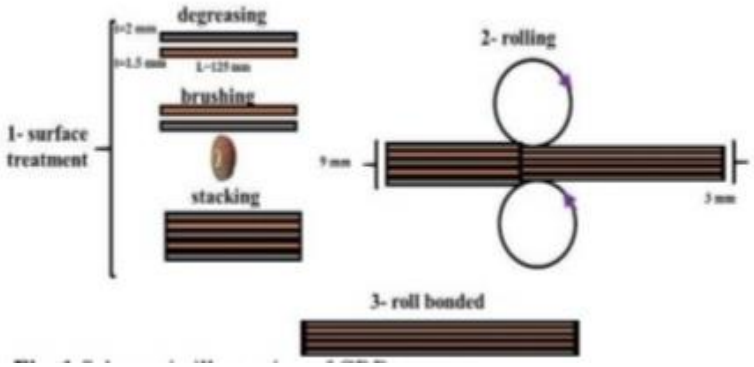

Figure 1. Schematic of the cold roll bonding process

Based on this, two magnesium sheets and three aluminum sheets were subjected to surface preparation treatments in order to remove surface contaminants. These treatments included washing with water and soap, degreasing using an acetone bath, and …

Mechanical brushing was also performed. The brushing process was carried out using a steel wire brush mounted on a bench drilling machine.

After the surface preparation process, two magnesium sheets and three aluminum sheets were stacked together in such a way that the aluminum sheets formed the outer surfaces of the composite, while the two magnesium sheets were placed between the aluminum layers. In order to prevent slipping between the stacked sheets, holes were drilled at the four corners of each sheet, and the sheets were tightly fastened together using steel wires. Subsequently, the rolling process was performed with an approximate thickness reduction of 70%.

Figure 2 presents images of the tensile test specimens after testing. Vickers microhardness tests were conducted separately for each layer under an applied load of 200 g with a dwell time of 10 seconds, measured along the direction perpendicular to the rolling direction.

Figure 2. Tensile test specimens after testing

The fracture surfaces of the specimens, after conducting the uniaxial tensile test, were examined using a scanning electron microscope (SEM) in order to investigate the quality of the roll-bonded interface between the layers and to determine the fracture mechanisms of the aluminum/magnesium composite produced by the roll bonding method. One of the specimens fractured at an angle of 45°, while the other specimen failed at an angle of 90°.

The detailed explanations for each specimen are provided in Section 1-6 (Fracture Analysis).

1-3 Forming Limit Diagrams

The Nakazima test mechanism is schematically illustrated in Figure 3. This test involves stretching the specimens until fracture using a hemispherical punch and a die, for samples with different lengths and widths.

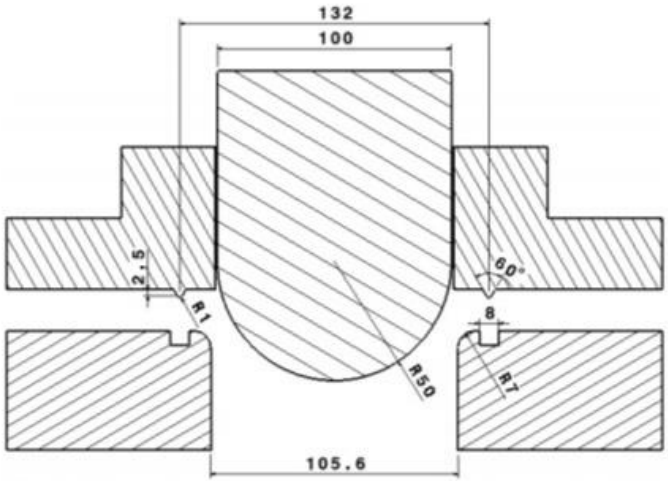

Figure 3. Schematic of the experimental setup for determining the forming limit diagrams

Nakazima Test

The principle of the Nakazima test is as follows: the sheet is clamped between the blank holder and the die, and then subjected to stretching by means of a hemispherical punch until a drop in force is observed in the force–displacement diagram, or in other words, until fracture occurs. Figure 4 illustrates the different stages of the Nakazima test.

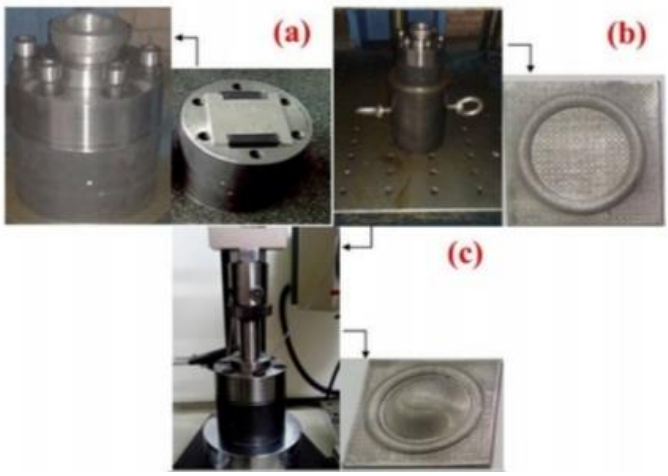

Figure 4. Equipment and different stages of the Nakazima test

For the forming limit diagram (FLD) test of the aluminum/magnesium composite, eight specimens were prepared using a wire-cut machine, in accordance with ISO 12004, as shown in Figure 5. The specimens had identical lengths and different widths, and a quarter-scale was employed due to the dimensions of the die and the fabricated samples.

Rectangular specimens were used to determine the right-hand side of the forming limit curve (uniaxial tension), while dog-bone-shaped specimens, similar to standard tensile test samples, were utilized to determine the left-hand side of the curve (biaxial tension).

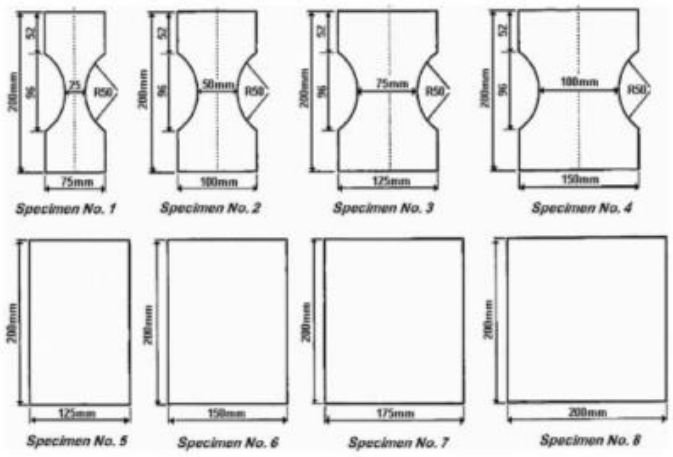

Figure 5. Geometry of different specimens for obtaining the forming limit diagrams

Forming Limit Diagram

The forming limit diagram defines the permissible range of principal strains prior to fracture and necking of the multilayer aluminum/magnesium composite for various forming processes, as discussed in Section 1-8 (Formability).

After performing the Nakazima test, the strains developed in the specimens were measured in order to plot the strain diagram. These measurements were carried out using a vernier microscope with an accuracy of 1 micrometer. After determining the values of *a* and *b*, which represent the major and minor diameters of the deformed ellipse, respectively, and using the initial diameter of the circle (*d*), the limiting engineering and true strain values were calculated based on the corresponding relationships.

1-4 Plastic Instability

Figure 6 presents optical microscopy images of the cross-section perpendicular to the rolling direction and in the longitudinal–thickness plane of the aluminum/magnesium composite produced by the cold roll bonding method.

As shown in Figure 6, severe plastic instability is observed in the magnesium layers. The main reasons for this plastic instability in the magnesium layers include the application of high strain during rolling, differences in flow properties and thickness between aluminum and magnesium, the imposition of mechanical working at room temperature, and the inherently low formability of magnesium. Nevertheless, as can be observed, the layered structure is preserved, and the magnesium reinforcing layers have not fractured throughout the entire specimen.

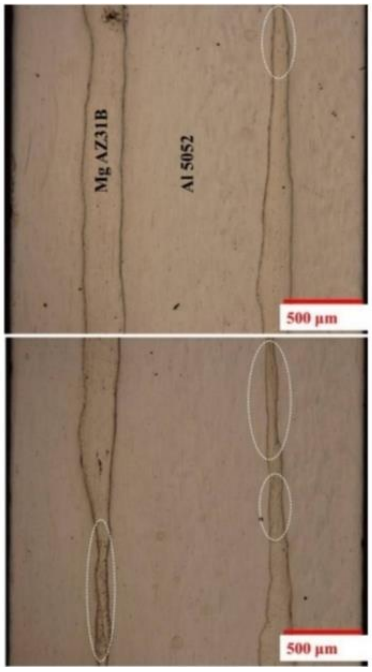

Figure 6. Microscopic images of the multilayer aluminum/magnesium composite produced by the cold roll bonding method

1-5 Results and Discussion

By selecting appropriate initial dimensions, applying proper surface preparation to the contacting layers, ensuring high formability, and minimizing the time interval between surface preparation and rolling in order to reduce surface oxidation, a strong interfacial bonding was achieved in the layered composites produced by the roll bonding method. In the present study, the application of a high strain (70% thickness reduction), the use of 5052 aluminum alloy with high formability, and appropriate surface preparation procedures played key roles in obtaining a sound bond at the composite interface

… as well as comprehensive surface preparation treatments, both chemical and mechanical, resulted in the formation of a strong bond that is free from discontinuities and delamination at the aluminum/magnesium interface.

1-6 Fracture Analysis

Magnesium, due to its hexagonal crystal structure, exhibits a completely brittle fracture behavior. The brittle fracture mechanism is characterized by the absence of micro-void formation and plastic deformation on the fracture surface, resulting in a smooth and uniform fracture surface, as also observed for magnesium in Figure 7.

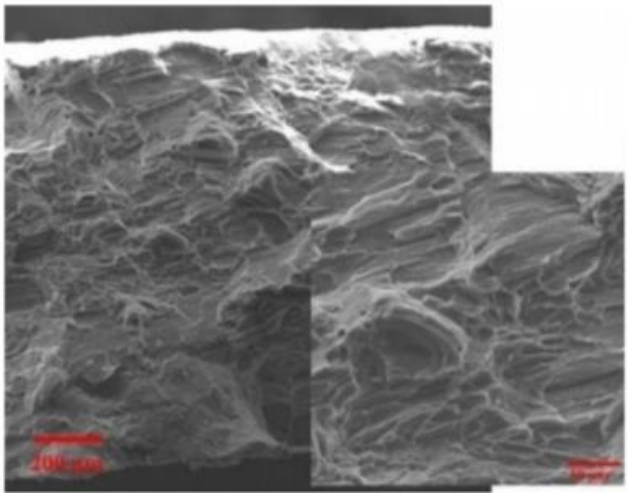

Figure 7. Fracture cross-section of AZ31B magnesium alloy

In Figure 8, equiaxed or hemispherical dimples are observed, which are characteristic features of ductile fracture. In metals with high toughness, the sizes of cracks and voids are considerably larger, and the growth and coalescence of these voids directly lead to fracture. In other cases, cracks are initiated and propagated as a result of the coalescence of micro-voids.

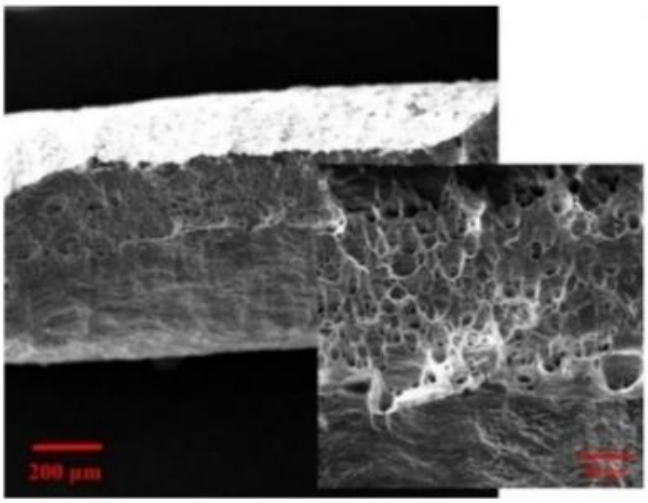

Figure 8. Fracture cross-section of aluminum alloy 5052

Figure 9 presents scanning electron microscope (SEM) images of the fracture cross-section of the aluminum/magnesium composite after the roll bonding process.

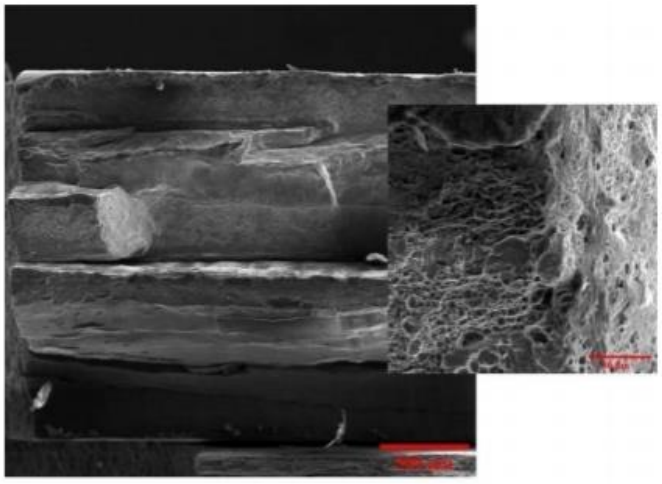

Figure 9. Fracture cross-section of the multilayer aluminum/magnesium composite produced by the cold roll bonding method

As can be observed, the presence of micro-voids and plastic deformation on the fracture cross-section confirms a ductile fracture behavior for the aluminum layers. However, compared to the initial aluminum material (prior to rolling), certain differences are evident, which are discussed below.

The tensile strength of the multilayer aluminum/magnesium composite after rolling reaches **273.5 MPa**, representing an improvement of **76%** and **89%** compared to the initial aluminum and magnesium samples, respectively. In contrast, the elongation to failure decreases significantly, reaching approximately **50%** for the multilayer aluminum/magnesium composite, which corresponds to reductions of more than **80%** and **70%** relative to the initial aluminum and magnesium specimens, respectively.

The primary reasons for this increase in strength and the concurrent reduction in elongation can be attributed to **cold working**, **severe thickness reduction (70%)**, and **work hardening induced by dislocation accumulation**. With the application of strain, the micro-voids become fewer in number and shallower, which, as previously mentioned, is a consequence of the reduced ductility and toughness of the aluminum layers after rolling.

1-7 Mechanical Properties

As can be observed, the aluminum alloy **5052** exhibits high strength and ductility, while magnesium also demonstrates adequate strength and formability. According to **Figure 10**, the multilayer aluminum/magnesium composite produced by the **roll bonding method**, consisting of **66.6% aluminum** and **33.3% magnesium**, exhibits a significantly higher strength than the initial materials; however, its ductility is severely limited.

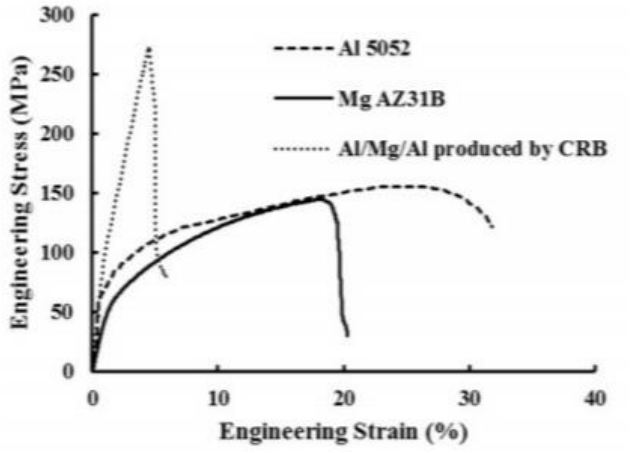

Figure 10. Engineering stress–strain curves for annealed samples and the bilayer aluminum sheet produced by the cold roll bonding method

Furthermore, **Figure 11** illustrates the variations in **Vickers microhardness** of the aluminum and magnesium layers in the composite produced by the **roll bonding process**, both **before and after rolling**. As can be observed, with the application of the rolling process, …

The Vickers microhardness of both the aluminum and magnesium layers increases significantly. The microhardness values of aluminum and magnesium rise from **79.9** and **63.4 HV** in the initial condition to **112.1** and **96.8 HV**, respectively, after the roll bonding process. These results indicate improvements of **41%** and **53%** in microhardness for the aluminum and magnesium layers, respectively.

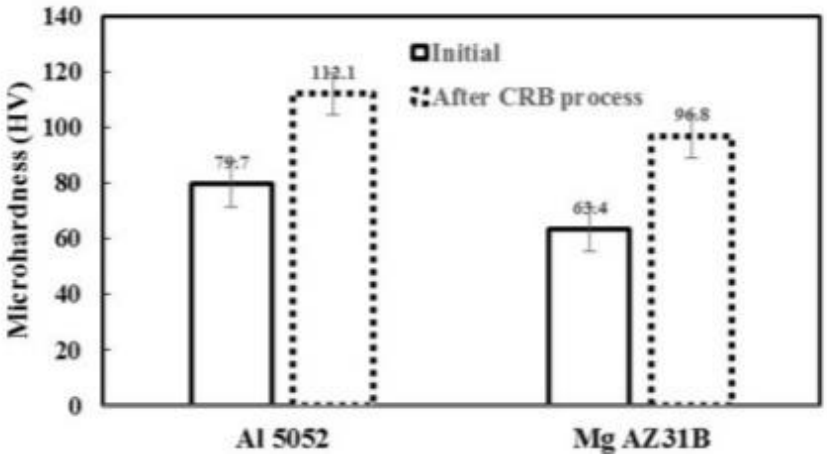

Figure 11. Vickers microhardness of the annealed sample and the bilayer aluminum sheet produced by the cold roll bonding method

1-8 Formability

The upper and lower surfaces of this curve define the range of **inadmissible strains** for forming operations. The **right-hand side** of the curve is obtained from **rectangular specimens** under a **tension–tension loading condition**, while the **left-hand side** is derived from **dog-bone–shaped specimens** subjected to **tension–compression loading**. The **lowest point of the curve** represents the allowable strains under **plane strain conditions** and, in effect, acts as the limiting factor for forming operations.

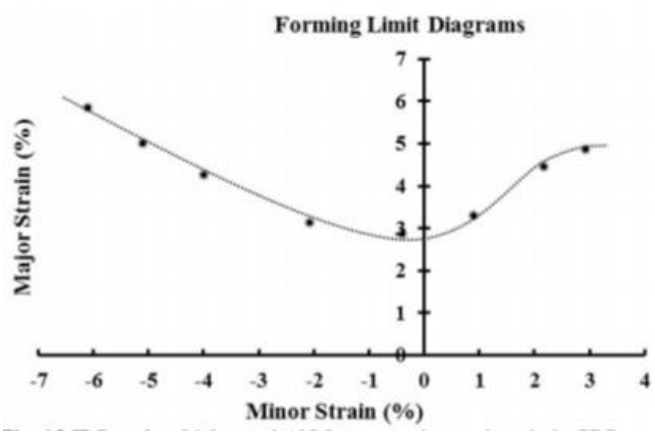

Figure 12. Forming limit diagrams (FLDs) of the multilayer composite produced by the cold roll bonding method

Chapter 2

2-1 Introduction

In this process, a tool consisting of a **pin and a shoulder** is plunged into the metallic sheet at a specified rotational speed. A groove is machined into the sheet, into which **ceramic particles** are introduced. The rotational motion of the tool over the sheet generates **frictional heat**, resulting in the **plasticization of the material**. The penetration of the pin into the sheet continues until the shoulder of the tool comes into contact with the surface of the sheet. Subsequently, the tool begins to move linearly along the predefined path, and after completing the traverse length, it is withdrawn from the sheet, thereby terminating the process.

Pumice powder with two different particle sizes (approximately **5 µm** and **100 nm**) was prepared by milling pumice stone using a **high-energy ball mill**, with a **ball-to-powder weight ratio of 10:1**, a **rotational speed of 300 rpm**, and milling times of **1 and 5 hours**.

The **7075 aluminum alloy**, due to its high **strength-to-weight ratio**, is widely used in **aerospace, military, marine, and automotive industries**. The fabrication of **aluminum matrix composites reinforced with ceramic particles** has consistently attracted the attention of design engineers because of their enhanced **creep strength**, **reduced coefficient of thermal expansion**, and improved **hardness and wear resistance**. One of the effective methods for producing such composites is the **friction stir processing (FSP) technique**. In this method, a rotating tool composed of a pin and a shoulder is plunged into the metallic sheet. A groove is created in the sheet and filled with ceramic particles. The rotational motion of the tool generates frictional heat, leading to material plasticization until the tool shoulder contacts the sheet surface. The tool then traverses linearly along the processing path and is finally retracted from the sheet, marking the completion of the process.

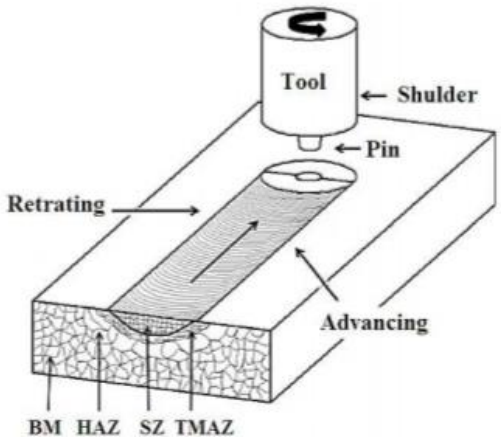

Figure 1. Schematic of the friction stir process (FSP)

In the present study, **micro- and nano-sized pumice particles** were employed to reinforce the surface of **7075 aluminum sheets** using the **friction stir processing (FSP) technique**. Pumice is a lightweight, porous volcanic stone rich in silica, which is abundantly available in Iran; therefore, it is inexpensive and its utilization is economically advantageous.

2-2 Materials and Experimental Procedure

To provide an appropriate **stir zone**, the **shoulder concavity angle** was set to **8°**, and the **tilt angle of the pin relative to the vertical axis** was fixed at **1°**. The **friction stir processing (FSP)** experiments were carried out using an **MK4FP milling machine** manufactured by **Tabriz Machine Manufacturing Company**. The specimens were securely clamped and fixed onto the milling machine using fixtures and vises, and were processed under specified **rotational and traverse speeds**.

Figure 2 shows the specimen clamped on the milling machine during the friction stir processing operation. The processing parameters used for sample fabrication are listed in **Table 1**.

Figure 2. Aluminum sheet being subjected to the friction stir process (FSP)

Rotational Speed (rpm)	Traverse Speed (mm/min)	Number of Passes	Experiment Number
800	80	1	1
800	40	1	2
800	40	4	3
1200	40	4	4
Experiment Number 4 with micro-sized pumice particles			5
Experiment Number 4 with nano-sized pumice particles			6

Table 1. Friction Stir Process Parameters

Prior to the fabrication of the composite specimens, a groove with a width of **1.5 mm** and a depth of **1.5 mm** was machined at the center of the **upper surface of the sheets** using a milling machine. The pumice powder was then introduced into the groove using a salt-shaker–type container, and the excess powder was removed from the surface. Subsequently, the groove was sealed using a **pinless tool** in order to prevent powder ejection during the composite fabrication process.

After completion of the processing, the **stir zone** was separated by **wire-cut machining**, and its cross-section was ground and polished. The prepared surface was then etched for **10 seconds** in a solution consisting of a mixture of **nitric acid, hydrochloric acid, and hydrofluoric acid**.

2-3 Results and Discussion

Figure 3 shows an **optical microscopy image** of the cross-section of **Sample 1** (single pass, **traverse speed of 80 mm/min**, **rotational speed of 800 rpm**). In this image, the **stir zone (SZ)**, **thermo-mechanically affected zone (TMAZ)**, **heat-affected zone (HAZ)**, and **base metal (BM)** are clearly identified.

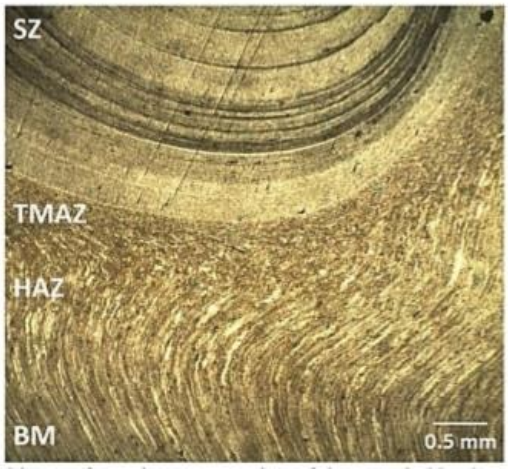

Figure 3. Optical micrograph of the cross-section of Sample 1

As shown in **Figure 4** and **Table 2**, reducing the **linear traverse speed** from **80 to 40 mm/min** (comparison of **Samples 1 and 2**) results in a **slight increase** in the average microhardness of the **stir zone**, from **80.2 to 82.0 Vickers**. Furthermore, by increasing the **number of processing passes** from **one to four passes** (**Sample 3**), the average microhardness increases to **86.7 Vickers**.

By increasing the **tool rotational speed** from **800 to 1200 rpm** (**Sample 4**), a more pronounced increase in microhardness is observed, reaching **94.6 Vickers**. This behavior can be attributed to variations in the **degree of material stirring and plastic deformation** induced by the **friction stir processing (FSP)** technique as a result of changes in the **number of passes**, **linear traverse speed**, and **tool rotational speed**.

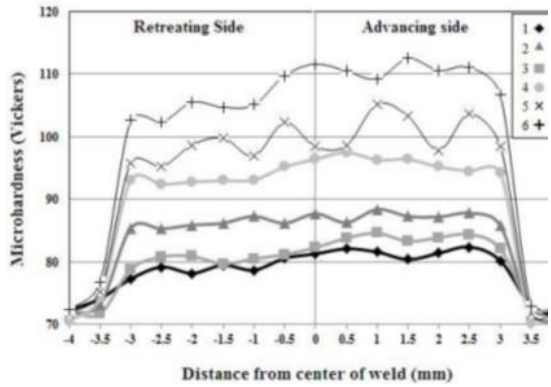

Figure 4. Microhardness results for the samples

Sample Number	Average Microhardness (Vickers)
1	80.2
2	82.0
3	86.7
4	94.6
5	99.6
6	107.8

Table 2. Average Microhardness in the Stir Zone

A comparison of the **microhardness values of Samples 4, 5, and 6**, as presented in **Figure 4** and **Table 2**, indicates that the **addition of pumice particles** leads to an increase in the microhardness of the **stir zone**. The average microhardness increases from **94.6 Vickers** to **99.6 Vickers** with the addition of **pumice microparticles**, and further increases to **107.8 Vickers** with the incorporation of **pumice nanoparticles**.

The variation in the degree of material stirring can be rationalized by its effect on **grain size**. In other words, with an **increase in the number of processing passes**, a **reduction in linear traverse speed**, and an **increase in tool rotational speed**, a more pronounced **grain refinement** occurs in the **stir zone**. **Figures 5 and 6** present the **optical microscopy** and **scanning electron microscopy (SEM)** images, respectively, of the cross-section of the stir zone in **Samples 1 and 4**.

The **grain size** was measured using the **distance measurement software integrated into the scanning electron microscope (SEM)**, based on the **average dimensions of 20 grains**. The grain size of **Sample 1** was approximately **10 µm**, which decreased to about **5 µm** in **Sample 2**.

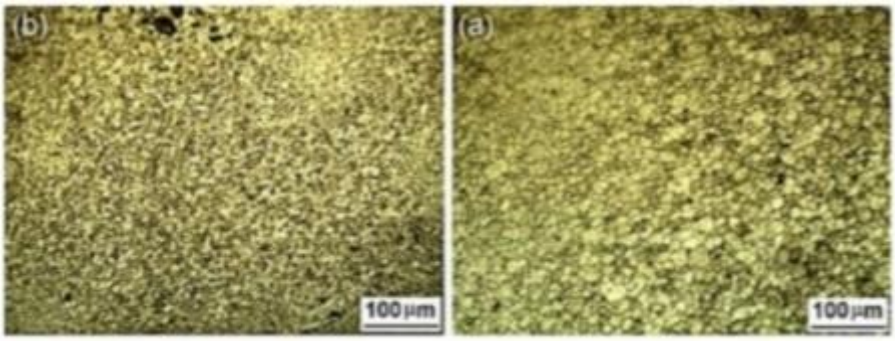

Figure 5. Optical micrograph of the cross-section of the stir zone for a) Sample 1 and b) Sample 4

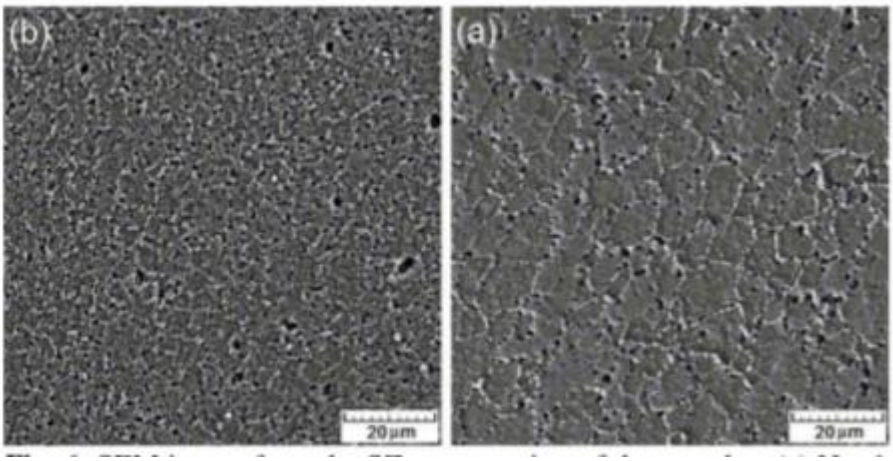

Figure 6. Scanning Electron Microscope (SEM) image of the cross-section of the stir zone for a) Sample 1 and b) Sample 4

The **dark spots observed in the microstructural images** correspond to **porosities** that were formed during the **stirring process**. The relationship between the **increase in hardness (H)** and the **reduction in grain size (D)** can be explained based on the **Hall–Petch relationship**. According to this relationship, H0 H_0 H0 and K K K are material-dependent constants that vary with the nature of the material.

$$H = H_0 + \frac{K}{\sqrt{D}}$$

Another noteworthy observation inferred from the **hardness profile in Figure 4** is that the **hardness of the composites in the advancing side** is **slightly higher** than that in the **retreating side**. In the advancing side, the **direction of tool rotation and the direction of tool traverse are the same**, whereas in the retreating side, they are **opposite**. Consequently, on the advancing side, the **stirring intensity**, **material flow**, and **distribution of ceramic powder particles within the matrix** are enhanced, leading to a **greater increase in hardness**. By increasing the **number of processing passes** and **altering the direction of tool rotation in each pass**, the **hardness difference between the advancing and retreating sides** can be reduced.

Chapter 3

Introduction to Composites and Aluminum Matrix Composites: Applications and Characteristics

The resulting **composite material** possesses a **combination of properties** that cannot be achieved by any of its individual constituent materials alone. According to the definition provided by the **American Society for Metals (ASM)**, a composite is a **macroscopic combination of two or more distinct materials** with a **well-defined interface** between them.

The constituent materials exhibit **completely different physical and chemical properties** and are combined to produce a material whose characteristics are **distinct from those of the individual components**. Within the newly formed material, these constituents **remain separate and distinguishable**, which differentiates **composites** from **mixtures and solid solutions**.

Advanced composites are, in the true sense of the term, **"engineered materials"**, meaning that an engineer can control both the **nature of the constituent materials** and their **physical arrangement** in order to fabricate materials with **highly specific and tailored properties**.

Characteristics of Aluminum Matrix Composites

Various metals are used as the **matrix phase** in metal matrix composites, among which **aluminum** is one of the most important. A wide range of aluminum alloys, in different forms, are employed in the fabrication of aluminum matrix composites. The reasons for the **cost-effectiveness and widespread application** of aluminum and its alloys include **low density**, **ease of fabrication**, and **favorable physical and mechanical properties**.

The density of most aluminum alloys is close to that of pure aluminum, which is approximately **2.7 g/cm^3**, corresponding to **about one-third of the density of steel, copper, or brass**. Aluminum exhibits **high corrosion resistance** in most environments, including air, water (or saltwater), petrochemical systems, and other chemical processing equipment. Moreover, aluminum possesses **excellent thermal and electrical conductivity**. In addition, its **non-magnetic nature** is considered an important advantage in **electrical and electronic industries**.

Aluminum alloys are generally classified into two main categories: **cast alloys** and **wrought alloys**.

Pure aluminum melts at approximately **660 °C**. This relatively low melting temperature, compared with other commonly used metallic matrices, facilitates the fabrication of **aluminum matrix composites (AMCs)** using **casting methods**. Among the advantageous properties of aluminum casting alloys are **good fluidity**, which enables the filling of thin sections, and **rapid heat transfer from the molten metal to the mold**, leading to increased casting cycle speeds.

Hydrogen is the **only gaseous element soluble in molten aluminum**, and its solubility can be readily controlled. Most aluminum alloys exhibit **low susceptibility to hot cracking and tearing**, are **chemically stable**, and produce a **satisfactory surface finish** after casting. Among aluminum casting alloys, **Al–Si alloys** are particularly prominent due to their **higher fluidity**, making them well suited for the production of **complex shapes and thin-walled components**. Therefore, **fluidity** is a key factor in selecting a castable composite matrix.

The main advantages of aluminum-based composites include:

1. **High mechanical strength-to-weight ratio**
2. **Excellent corrosion resistance**
3. **Superior fatigue properties compared to conventional metals**
4. **High volume-to-weight efficiency**
5. **Lightweight nature, in some cases offering several times the strength of steel at a fraction of its weight**
6. **Lower cost and economic efficiency**
7. **High overall strength**

The improved **fatigue performance** of composite materials compared with conventional metals is attributed to their **multi-constituent nature**, in which each component contributes independently to fatigue resistance. In addition, **rolling processes** promote **grain elongation along the rolling direction** and significant thickness reduction, which enhances fatigue performance. Furthermore, the presence of **composite microparticles** contributes to material strengthening.

Advantages of Aluminum Matrix Composites

In aluminum matrix composites, **aluminum or aluminum alloys** are used as the **matrix phase**, while **non-metallic reinforcements**—most commonly **ceramic particles such as SiC and Al_2O_3**—serve as the **secondary phase**. The major advantages of aluminum matrix composites include:

• **The ability to achieve higher strength**

Additional advantages of aluminum matrix composites include:

• **Improved properties in high-temperature applications**

• **Control of the coefficient of thermal expansion**

• **Enhanced electrical performance**

• **Improved wear resistance**

• **Mass control, particularly in cyclic loading applications**

To better understand the significance of these composites, their advantages can be demonstrated quantitatively through specific examples. For instance, the use of **60 wt.% continuous Al_2O_3 fibers** as reinforcement in a pure aluminum matrix results in an increase in the **elastic modulus from approximately 70 GPa to 240 GPa**. Furthermore, research findings indicate that the **wear resistance of a composite containing 20 vol.% SiC particles in an Al–9%Si matrix** is comparable to, or even higher than, that of **gray cast iron**. These examples clearly demonstrate that the industrial properties of aluminum and its alloys can be **significantly enhanced** through the incorporation of an appropriate **volume fraction of reinforcement**.

Aluminum matrix composites provide a **unique combination of properties** that cannot be matched by conventional aluminum alloys. As a result, these composites are currently employed across a wide range of **engineering applications**. One of the key factors contributing to the attractiveness of these materials is their **high performance**, **environmental benefits**, and **economic advantages**.

In the transportation sector, the primary benefits of utilizing aluminum matrix composites include **reduced fuel consumption** and **lower noise levels**. With the implementation of increasingly stringent environmental regulations and a growing emphasis on performance optimization, these composites demonstrate strong potential to **replace monolithic materials** such as conventional aluminum alloys, ferrous alloys, titanium alloys, and even **polymer matrix composites** in many applications.

In recent years, the replacement of monolithic materials with aluminum matrix composites in engineering systems has undergone significant development, to the extent that **redesigning entire systems** to achieve reductions in **weight and volume** has become essential. According to the **American Science and Technology Association**, aluminum matrix composites can be regarded not only as **suitable substitutes for existing materials with superior performance**, but also as materials capable of enabling **fundamental changes in product and system design**.

Moreover, by employing **near-net-shape manufacturing processes** and selecting appropriate reinforcements, the use of aluminum matrix composites can provide **economically viable solutions** for a wide range of commercial applications. Consequently, the application of aluminum matrix composites in various transportation sectors is expected to be **highly desirable and, indeed, inevitable in the coming years**.

Chapter 4

Fabrication Methods of Aluminum Matrix Composites

The fabrication methods of aluminum matrix composites can generally be classified into two main categories: **solid-state processes** and **liquid-state processes**.

4-1 Solid-State Processes

4-1-1 Powder Metallurgy (PM)

In this method, **fine oxide particles** act as **strengthening agents**. These particles often have a significant influence on the **purity of the matrix**, particularly during **heat treatment operations**. Powder metallurgy enables relatively good control over the microstructure; however, contamination and oxide formation may affect the final properties of the composite.

4-1-2 Diffusion Bonding

Diffusion bonding is a **highly demanding and labor-intensive process**. Achieving a **high volume fraction of fibers** as well as a **homogeneous fiber distribution** using this method is extremely difficult. As a result, although diffusion bonding can produce high-quality interfacial bonding, its industrial application is limited.

4-1-3 Physical Vapor Deposition (PVD)

In the **physical vapor deposition (PVD)** process, composite fabrication is completed by placing **coated fibers** within the matrix phase or by **aligning the fibers** and consolidating them through **hot pressing** or **hot isostatic pressing (HIP)**. Using this technique, composites with a **uniform fiber distribution** and **very high volume fractions (up to 80%)** can be produced. Despite its excellent control over microstructure, this method is generally expensive and limited to specialized applications.

4-2 Liquid-State Processes

4-2-1 Infiltration Process

The **metal infiltration process** is one of the most effective methods for producing **metal matrix composites with high reinforcement volume fractions** (greater than **50%**). This process is also considered **economically efficient**. Infiltration enables the fabrication of composite materials that are **difficult or impossible to produce using other techniques**.

The different types of metal infiltration processes include:

Pressureless Infiltration

Pressureless infiltration is, in comparison with other fabrication methods, **simpler and less expensive**. In this process, infiltration occurs **spontaneously**, without the application of any external force.

The disadvantages of this method include:

1. **Undesirable chemical reactions**
2. **Low process speed**
3. **The presence of porosity in the composite material**

Mechanical Pressure Infiltration

In **mechanical pressure infiltration**, the application of **high pressure** can provide several advantages, including **an increased processing rate**, **refinement of the matrix microstructure**, and **the production of defect-free components**. This method also makes it possible to **cast reactive metals** and to **manufacture complex geometries**.

Gas Pressure Infiltration

In **gas pressure infiltration**, the **infiltration time is shorter**, which improves the efficiency of the process.

Vacuum Infiltration

Vacuum infiltration of alumina fibers using a Li–Al alloy is an example of this method, in which infiltration occurs as a result of the **reduction reaction of alumina by lithium**.

Stir Casting

Stir casting is the **simplest and most commercially used method** for the production of **aluminum matrix composites**. The **low cost**, **simplicity of the process**, **material versatility**, and the **ability to fabricate large components** are among the main advantages of this technique.

In-Situ Process

In the **in-situ process**, the **reinforcement phase is formed within the molten matrix** through controlled **metallurgical and chemical reactions**. The resulting composites exhibit **desirable characteristics**, such as **better compatibility between the reinforcement and the matrix**, **finer reinforcement particles**, and a **more uniform particle distribution**.

Chapter 5

Conclusion

In **Paper 1**, optical microscopy images of the aluminum/magnesium composite demonstrated that a strong and continuous metallurgical bond was successfully formed at the aluminum–magnesium interfaces, with no observable delamination or separation between the layers. Moreover, the aluminum matrix of the Al/Mg composite fabricated through the roll-bonding process exhibited a ductile fracture behavior, characterized by smaller and shallower micro-voids compared to those observed in the initial material.

The results of the Vickers microhardness tests indicated a substantial increase in microhardness in both the aluminum and magnesium layers. The main factors responsible for the observed enhancement in strength and microhardness, as well as the reduction in elongation, can be attributed to cold working, the high thickness reduction ratio (70%), and strain hardening caused by increased dislocation density. In addition, forming limit diagrams (FLDs) are considered one of the most practical methods for determining the allowable strain ranges of different materials and are widely employed to assess the feasibility of various sheet-metal forming processes.

In **Paper 2**, the results showed that reducing the linear traverse speed, increasing the number of processing passes, and increasing the tool rotational speed led to a reduction in grain size within the stir zone, which consequently resulted in improved hardness and wear resistance. Under identical friction stir processing conditions, composite samples reinforced with micro- and nano-sized pumice particles exhibited significantly higher hardness and wear resistance compared to the non-composite sample. Furthermore, the effect of nano-scale particles on enhancing hardness and wear resistance was found to be more pronounced than that of micro-scale particles.

References

1. **Article 1:**

   Investigation of the Formability of a Multilayer Composite Processed by the Roll Bonding Method.

2. **Article 2:**

   Composite Fabrication and Surface Reinforcement of Aluminum 7075 Using Micro- and Nano-Sized Pumice Particles by the Friction Stir Processing (FSP) Method.

3. **Book:**

   Methods of Manufacturing Aluminum Matrix Composites,

   Dr. Abbas Honarbakhsh.

4. **Website:**

   www.fa.m.wikipedia.org